14th International Symposium on Turbulence and Shear Flow Phenomena (TSFP14)
Heidelberg, Germany, July 28–31, 2026

VELOCITY-STRESS SCALE-DEPENDENT ADMITTANCE FOR TURBULENCE OVER TEXTURED SURFACES

Joy Chen
Dept of Engineering, U of Cambridge
Cambridge CB2 1PZ, UK
jc2392@cam.ac.uk

Guilhem Cabannes
School of Engineering, EPFL,
1015 Lausanne, Suisse
Dept of Engineering, U of Cambridge,
Cambridge CB2 1PZ, UK
guilhem.cabannes@epfl.ch

Zengrong Hao
Dept of Engineering, U of Cambridge
Cambridge CB2 1PZ, UK
zh343@cam.ac.uk

Ricardo García-Mayoral
Dept of Engineering, U of Cambridge
Cambridge CB2 1PZ, UK
r.gmayoral@eng.cam.ac.uk

ABSTRACT

This work presents a framework for modelling the influence of surface texture on turbulent flows using lengthscale-dependent admittance coefficients, which relate velocity to stress at the free-flow/substrate interface. The asymptotic homogenisation approach assumes scale separation between texture and flow, but this breaks down for texture sizes relevant to most turbulent applications. We instead consider the distinct flow responses to velocity excitations of different scales, computing admittance coefficients as a function of wavelength. The framework is applied to rough and porous substrates with flow governed by steady or unsteady Stokes. We show that inertia, as captured by the unsteady formulation, is essential for accurately representing the DNS-measured coefficient in both magnitude and phase. The resulting admittances are implemented as equivalent boundary conditions in simulations that do not explicitly resolve the texture, and are shown to accurately recover the turbulent dynamics observed in texture-resolved DNS. In addition, we conduct a systematic assessment of individual admittance coefficients to gain physical insight into the relative importance of the different mechanisms they capture. By selectively retaining each coefficient in isolation, we show that the pressure-driven transpiration effect plays the most dominant role. For sufficiently deep porous and rough substrates, the transpiration contribution alone is sufficient to capture the primary effects of the texture on the turbulence.

Introduction

Turbulent flow over textured surfaces is ubiquitous in engineering applications and environmental flows. Investigating such flows typically requires extensive experimental campaigns or texture-resolved direct numerical simulations (DNSs), both of which are very expensive. This work proposes a framework to model the influence of surface texture on the overlying flow using lengthscale-dependent admittance coefficients, which relate velocity and stress at the free-flow/substrate interface. By avoiding the need to explicitly resolve the textures, this approach significantly reduces the resolution required and the computation cost, while providing physical insight into the effect of textures on the overlying turbulence.

A popular approach of obtaining admittance coefficients uses asymptotic homogenisation, which leverages the separation of scales between the microscale texture size (L) and the macroscales in the flow above (H), i.e. $\varepsilon = L/H \ll 1$. First-order homogenisation leads to a tensorial relation between the wall-parallel velocity and shear stress (Luchini *et al.*, 1991; Lauga & Stone, 2003; Kamrin *et al.*, 2010; Luchini, 2013). Higher-order expansion additionally incorporates the pressure and wall normal velocity, hence allowing non-zero transpiration at the interface (Lācis *et al.*, 2020; Bottaro & Naqvi, 2020; Naqvi & Bottaro, 2021; Sudhakar *et al.*, 2021; Luchini & Chung, 2026). While this method works well for small textures and laminar flows where $\varepsilon \ll 1$, they become inadequate in turbulent applications. The smallest scale of near-wall turbulence is the width of the quasi-streamwise vortices, which is around 15 wall units (Blackwelder & Eckelmann, 1979). Therefore, textures of sizes $L^+ \gtrsim 10$ will not satisfy scale separation, and this size range spans all but the hydraulically smooth regime.

To address this limitation, Hao & Garcia-Mayoral (2022) proposed a framework that considers the texture response to excitations of finite wavelength, as illustrated in figure 1. Building on this approach, the present work computes admittance coefficients from the flow response to excitations of a range of wavelengths, using the steady- and unsteady-Stokes formulation for rough and porous substrates by Hao & García-Mayoral (2025).

Gómez-de-Segura & García-Mayoral (2019) performed simulations in which the admittance relationship of textured surfaces is imposed as boundary conditions to model their effects without resolving the textures. In the present work, we revisit this technique and apply the admittance coefficients obtained with the new framework as the boundary condition. This provides a proof of concept for assessing whether the proposed framework can reproduce the key turbulent dynamics. Thus, this allows us to validate both the computed admittance coefficients and their use in reduced-order modelling, while

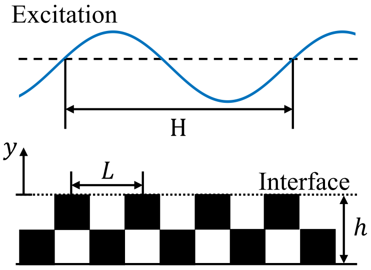

Figure 1. Sketch of the finite-wavelength excitation method to obtain the admittance coefficients for an excitation of scale H and for a texture of pitch L.

providing physical insight into the effect of textures on the flow.

Admittance model for surface texture

Asymptotic homogenisation at second order or above can be expressed as the velocity-stress relationship in the form of

$$\begin{bmatrix} u \\ v \\ w \end{bmatrix}_{y=0} = \mathbf{H} \begin{bmatrix} \partial_y u \\ p \\ \partial_y w \end{bmatrix}_{y=0}, \quad (1)$$

where x, y and z are the streamwise, wall-normal and spanwise coordinates, respectively, and u, v, w are their corresponding velocity components. The admittance matrix $\mathbf{H}$ includes terms of different homogenization orders, $\mathrm{O}(\varepsilon), \mathrm{O}(\varepsilon^2)$, etc. The interface, $y = 0$, is defined at the tip of the texture.

The admittance coefficients can be examined on a scale-by-scale basis by expressing the velocities and stresses as Fourier coefficients associated with a single wavenumber $\boldsymbol{k} = [k_x, k_z]$. In a coordinate system aligned with the wavevector $\boldsymbol{k}$, equation 1 reduces, for isotropic textures, to

$$\begin{bmatrix} \hat{u}_{\parallel} \\ i\hat{v} \\ \hat{u}_{\perp} \end{bmatrix}_{y=0} = \begin{bmatrix} \mathscr{L}_{slip} & k\mathscr{K}_{slip} & 0 \\ k\mathscr{N}_{trsp} & k\mathscr{K}_{trsp} & 0 \\ \sim 0 & \sim 0 & \mathscr{L}^{\perp}_{slip} \end{bmatrix} \begin{bmatrix} \partial_y \hat{u}_{\parallel} \\ -i\nu^{-1}\hat{p} \\ \partial_y \hat{u}_{\perp} \end{bmatrix}_{y=0}, \quad (2)$$

where $u_{\parallel}$ and $u_{\perp}$ are the velocity components along the $y = 0$ plane, parallel and perpendicular to the wavevector, respectively, ν is the kinematic viscosity, $k = |\boldsymbol{k}|$, and hatted variables denote quantities in Fourier space. Notably, $\mathscr{L}_{slip}$ and $\mathscr{L}^{\perp}_{slip}$ represent slip lengths, while $\mathscr{K}_{trsp}$ quantifies the coupling between pressure fluctuations and transpiration.

To illustrate the implications of the breakdown of homogenisation in turbulent applications, figure 2(a) presents the variation of the magnitude of the transpiration coefficient $\mathscr{K}_{trsp}$ with streamwise wavelength for spanwise uniform waves, $k_z = 0$. The shallow porous substrates consisting of two layers of staggered cubes from Hao & García-Mayoral (2025) with sizes $L^+ = 12$, 24 and 36 are used here as a representative example. Best-fit correlations measured from DNSs following the method of Hao & Garcia-Mayoral (2022) are included in the figure and serve as the reference against which all models are compared. First-order homogenisation cannot account for transpiration effects, yielding a zero $\mathscr{K}_{trsp}$. Second-order homogenisation likewise yields zero transpiration for an impermeable substrate floor, but permits non-zero transpiration when a Darcy transpiration is imposed at the substrate floor (Naqvi & Bottaro, 2021). This simply transfers the bottom Darcy transpiration to the admittance, yielding a constant $\mathscr{K}_{trsp} = K_{Darcy}$, which deviates significantly from the values measured from DNS. Third-order homogenisation following Bottaro & Naqvi (2020) results in a lengthscale-dependent $\mathscr{K}_{trsp}$, which is asymptotically correct at large wavelengths but diverges from the DNS measurements when $\lambda_x/L \lesssim 10$. The Darcy-Brinkman model of Gómez-de-Segura & García-Mayoral (2019) also shows good agreement at large λ_x/L and captures the overall trend qualitatively, but exhibits similar deviations quantitatively at smaller scales.

For all the textures considered, the pressure fluctuations in near-wall turbulence that trigger the transpiration effect have typical lengthscales of $\lambda^+ \approx$ 150-250, where $\lambda = 2\pi/k$, similar to those of smooth-wall flows (Hao & García-Mayoral, 2025), as highlighted in the figure. The accuracy of $\mathscr{K}_{trsp}$ is therefore critical in this range. However, both homogenisation and the Darcy-Brinkman model fail to provide accurate predictions in this region, and the predictions worsen as the texture size increases.

The breakdown of scale separation is also evident in the phase of the admittances, as portrayed in figure 2(b). All models discussed thus far yield a zero phase, suggesting that v and p are in sync, as opposed to the sizable v-p phase offset observed in DNS.

To overcome these limitations, we adopt the framework proposed by Hao & Garcia-Mayoral (2022), in which the admittance coefficients are obtained from the flow response to finite-wavelength excitations of the form $u_e = e^{i\boldsymbol{kx}}$. The problem is solved independently for each excitation wavenumber, yielding a scale-dependent description of the interface behaviour. This procedure avoids any assumption of scale separation between the texture and the flow, and therefore remains applicable even when the excitation wavelength is no longer much larger than the texture size.

We solve the flow response using governing equations of increasing complexity. Steady Stokes is the standard equation used in the homogenisation method and is also assumed in the Darcy-Brinkman model. The assumption of vanishingly small textures means that the Reynolds number $Re \to 0$, and viscous effects dominate in the flow. Upon Fourier transformation of the steady-Stokes equation in x, z and t, the governing equations are purely real, e.g. the viscous term is proportional to $-k^2$, resulting in the admittance coefficients exhibiting no phase shift. This explains why all models thus far systematically predict zero phase.

Non-zero phase arises from inertial or advective effects, associated with $\partial/\partial t$ and $\boldsymbol{u} \cdot \nabla$ in the governing equations. These introduce imaginary contributions proportional to $i\omega$ or ik, enabling phase shifts between excitation and response. To include this additional effect, we extend the governing equation to unsteady Stokes. The unsteadiness is introduced by a travelling excitation $u_e = e^{i(\boldsymbol{kx}-\omega t)}$. The angular frequency ω is determined by assuming a streamwise phase speed $c^+ = \omega^+/k_x^+ = 10 - \Delta U^+$, representative of the mean advection for near-wall turbulence (Del Álamo & Jiménez, 2009). We have also considered the addition of linearised advection, but the results are very similar to the unsteady-Stokes model. This is also consistent with the order of magnitude analysis done by Hao & Garcia-Mayoral (2022), which suggests that the temporal term dominates over the advective term. Thus, we restrict our attention to the steady- and unsteady-Stokes model.

Admittance coefficients are computed using the present formulation and validated against measurements from fully re-

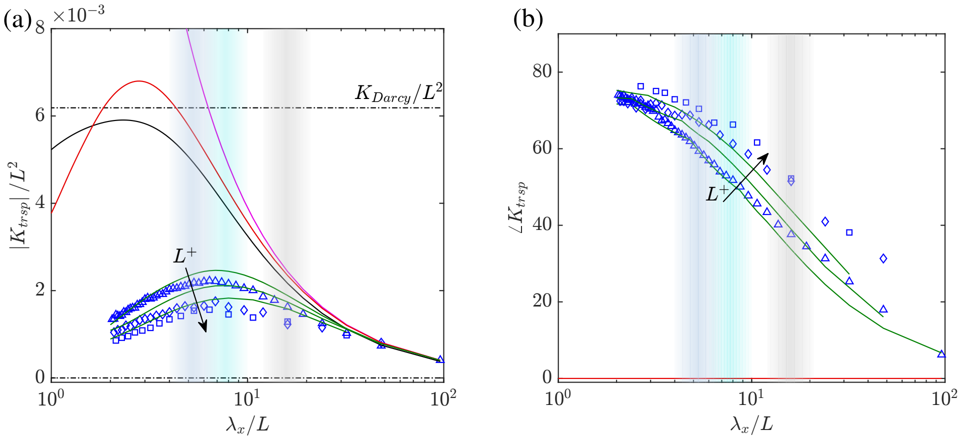

Figure 2. Normalised admittance coefficient $\mathscr{K}_{trsp}/L^2$ as a function of the normalised streamwise wavelength λ_x/L for a shallow porous substrate with inclusions of pitch L; (a) magnitude, (b) phase in degrees. △, ◊, □, values obtained from a fit of the texture resolved DNS data from Hao & García-Mayoral (2025), corresponding to substrates with $L^+ = 12$, 24 and 36, respectively. In (a), $- \cdot -$ at $K_{trsp} = 0$ and $\mathscr{K}_{trsp}/L^2 = K_{Darcy}/L^2 \approx 6.2 \cdot 10^{-3}$ correspond to second-order homogenization with an impermeable floor and a transpirable floor with permeability K_{Darcy}, respectively. ——, prediction from a Darcy-Brinkman model; ——, third-order homogenisation; ——, steady-Stokes coefficients; ——, unsteady-Stokes coefficients. Grey, cyan, and blue shaded regions represent, for substrates with $L^+ = 12$, 24 and 36, respectively, the dominant scales for turbulent pressure fluctuations, $\lambda^+ \approx 150$-250.

solved DNS data of Hao & García-Mayoral (2025) for rough (Ro), shallow porous (Ps), and deep porous (Pd) configurations, comprising one, two, and five or more layers of staggered cubes. Texture sizes of $L^+ = 12$, 24, 36 and 48 are considered with a fixed gap-to-pitch ratio $g/L = 0.5$, where g is the gap between cubes and L the grain pitch. Cases are denoted as, for example, 'Ro-12', where the prefix 'Ro' indicates the substrate configuration and the suffix '12' the grain pitch L^+.

Results for admittance coefficients

Using the shallow porous case Ps-12 as a representative example, the five admittance coefficients in equation 2 are portrayed for different wavenumbers in figures 3 and 4. The former presents the coefficients over the range of two-dimensional wavelengths considered, while the latter presents one-dimensional cuts at $k_x = 0$ and $k_z = 0$ for easier visual comparison of data. The DNS measured coefficients are only presented for $\lambda_x, \lambda_z \geq 2L$, as texture coherent flow introduces significant noise to the admittance at smaller wavelengths (Fairhall *et al.*, 2019). For larger textures, this restriction excludes a substantial portion of the DNS data, limiting the usefulness of the comparison; therefore, the $L^+ = 12$ case is presented here, as a sufficiently broad range of scales is retained. We leave for future work the measurement of admittance from DNS flow fields with the texture-coherent flow filtered out.

Admittances from the steady-Stokes model exhibit symmetry between the streamwise and spanwise directions for isotropic textures, resulting in identical values for the corresponding modes as portrayed in figure 3, but this symmetry is broken in the unsteady-Stokes model. This is also observed in figure 4, where the steady-Stokes solution yields identical behaviour for streamwise- and spanwise-uniform modes. For isotropic textures, stationary waves oriented in either direction are identical. In the unsteady-Stokes model, however, the frequency ω decreases with increasing wave inclination relative to x, as c^+ in the wave direction is the projection of the streamwise wavespeed. Thus, streamwise-uniform waves do not exhibit temporal variation and reduce to the steady-Stokes solution.

Overall, the steady-Stokes model shows significant deviations from the DNS data in both magnitude and phase, whereas the unsteady-Stokes model captures the trends in both. These results for spanwise uniform waves are also included in figure 2, where the steady-Stokes model exhibits behaviour similar to the Darcy-Brinkman model, with significant discrepancies emerging for $\lambda_x/L \lesssim 10$. In contrast, the unsteady model provides a substantial improvement in this region.

Despite the improvement from the inclusion of inertia, discrepancies with DNS measurements remain, particularly for $\mathscr{L}_{slip}$ and $\mathscr{L}_{slip}^{\perp}$. We do not yet fully understand the origin of this discrepancy, but likely contributions include noises due to the texture-coherent flow on the DNS measurements and the absence of nonlinear effects in the unsteady-Stokes model. Given the discrepancies and uncertainties of both the DNS-measured admittances and the ones from the unsteady-Stokes model, we consider both sets of coefficients in the textureless simulations discussed next, and assess the ability of either set to reproduce the turbulent dynamics observed in texture-resolved DNS.

Textureless simulations

We conduct DNSs of turbulent channel flows in a domain doubly periodic in the wall-parallel directions, using a code adapted from Gómez-de-Segura & García-Mayoral (2019). The admittance relation in equation 1 is introduced as equivalent boundary conditions at the channel walls to model the effect of the surface texture. Simulations are all conducted at friction Reynolds number $Re_\tau = \delta u_\tau/\nu \approx 180$, matching the value for the texture-resolved DNS. The channel is of size $[L_x, L_z, L_y] = [2\pi\delta, \pi\delta, 2\delta]$. A spectral discretisation is used in the streamwise and spanwise directions, while the wall-normal direction is discretised using second-order finite differences on a staggered grid. The wall normal grid is stretched, with $\Delta y^+_{min} \approx 0.3$ near the wall and $\Delta y^+_{max} \approx 3$ in the centre of the channel. The wall-parallel resolutions are $\Delta x^+ \approx 6$ and $\Delta z^+ \approx 3$. The temporal integration uses a fractional-step Runge-Kutta discretisation, where pressure is corrected to enforce incompressibility. A semi-implicit scheme is used for the viscous terms and an explicit scheme for the advective terms.

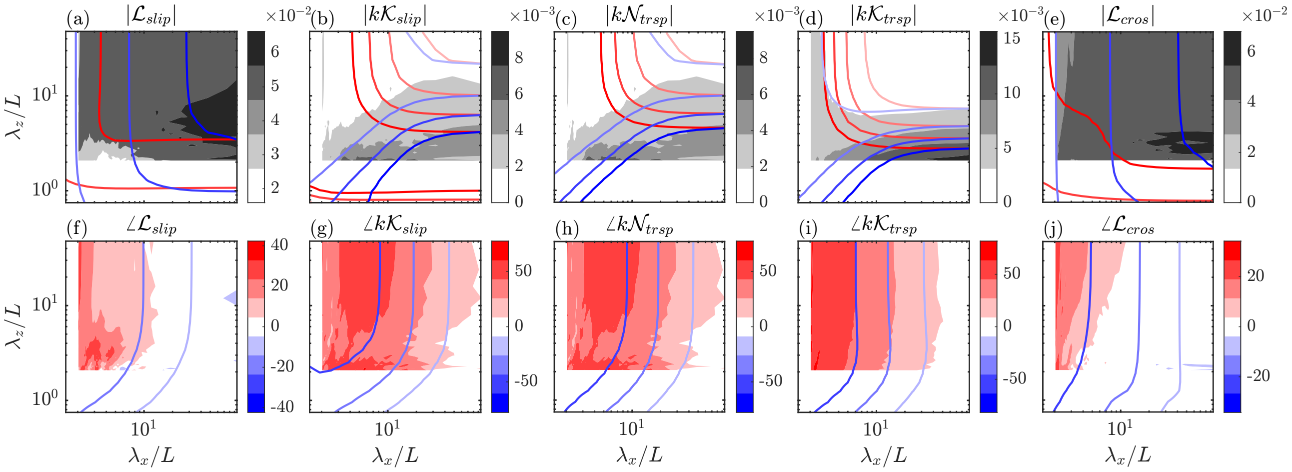

Figure 3. Admittance coefficients in wavenumber for Ps-12. (a-e), absolute value, and (f-j), phase in degrees. Shaded contours, values measured from texture-resolved DNS; —— and ——, results from steady- and unsteady-Stokes models, respectively, with colours varying from light to dark as the contour level increases. DNS-measured values are presented only for $\lambda_x, \lambda_z \geq 2L$. The phases for the coefficients from the steady-Stokes model are all zero.

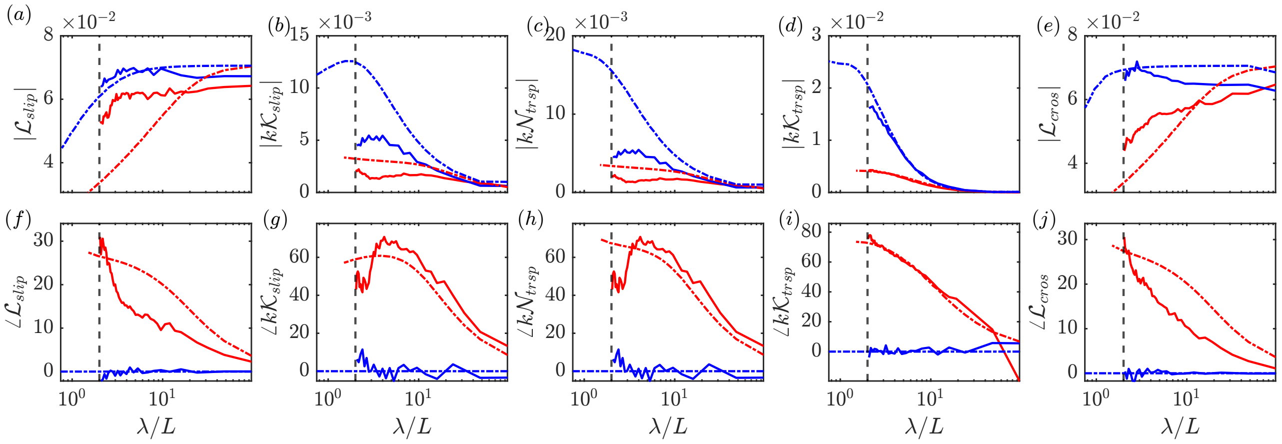

Figure 4. Admittance coefficients in wavenumber coordinates for case Ps-12 of figure 3. ——, spanwise uniform modes $k_z = 0$, and ——, streamwise uniform modes $k_x = 0$. ——, DNS measured values; $- \cdot -$, unsteady Stokes. Spanwise varying coefficients from unsteady Stokes, $- \cdot -$, coincide with the steady-Stokes coefficients in both directions. The dashed vertical line represents $\lambda/L = 2$.

Results for textureless DNS

Case Ps-24 is used as an example here, rather than Ps-12, since the latter remains close to smooth-wall behaviour and shows little sensitivity to the choice of coefficients, while the larger texture produces more pronounced differences, both compared with the smooth wall and across different models.

The mean and fluctuation profiles from the simulation using steady-Stokes admittances show significant disagreement with the texture-resolved DNSs, as portrayed in figure 5. This is consistent with the discrepancy in the corresponding coefficients. In contrast, the use of both the unsteady-Stokes and DNS-measured admittance recovers accurate flow statistics. The statistics from simulations with DNS-measured coefficients appear to deviate slightly more than the unsteady-Stokes case. This may indicate that the noise introduced by the texture-coherent flow is the main cause of the deviation between the two sets of coefficients, and the unsteady-Stokes model provides a more accurate representation in this case. A detailed investigation of this discrepancy is left for future work. Accordingly, hereafter we restrict the discussion to simulations employing the unsteady-Stokes coefficients.

The agreement between simulations using the unsteady-Stokes coefficients and the measurements from texture-resolved DNSs is observed across all the cases considered. Figures 6 and 7 portray the results for rough and deep porous substrates, respectively. At $L^+ = 24$, the profiles are in excellent agreement, but deviations emerge at the larger textures with $L^+ = 48$, resulting in an error of around 15% in the roughness function ΔU^+. Fairhall *et al.* (2019) attributed this degradation with increasing texture size to the growing influence of the texture-coherent flow, whose effect we do not model in our simulations, as the nonlinear interactions associated with this component modify the background turbulence. Modelling larger textures, therefore, will likely require additional forcing terms to account for these effects, as done in Xie *et al.* (2024). The agreement between texture-resolved DNS and textureless simulation can also be seen from the spectra portrayed in figure 8, using the case Pd-48-50 as an example. Even at the large texture size of $L^+ = 48$, the textureless simulation agrees well with the DNS results. At a smaller texture size of $L^+ = 24$ and 12, the agreement is nearly exact.

To gain physical insight into the relative importance of the different admittance coefficients, we have also conducted a series of textureless simulations in which individual coefficients

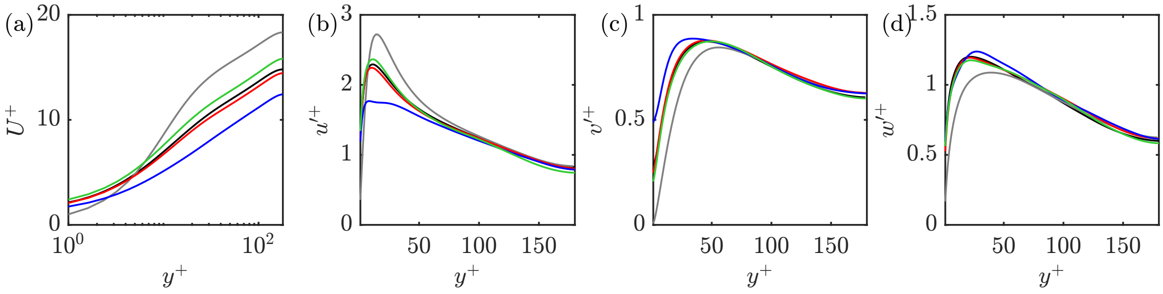

Figure 5. (a) Mean flow profile, (b-d) r.m.s of velocity fluctuations of Ps-24 simulations. ——, texture-resolved DNS from Hao & García-Mayoral (2025); ——, textureless simulation using DNS measured admittance coefficients; ——, steady-Stokes coefficients; ——, unsteady-Stokes coefficients; ——, reference smooth wall data.

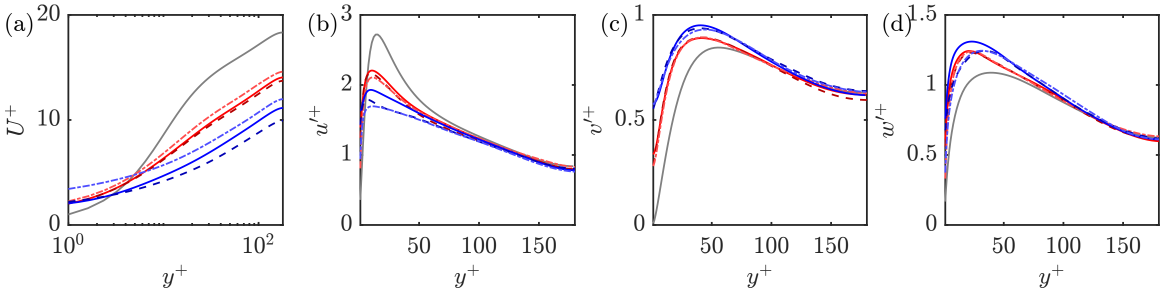

Figure 6. (a) Mean flow profile, (b-d) r.m.s of velocity fluctuations of simulations for deep porous textures. ——, $L^+ = 24$; ——, $L^+ = 48$; ——, reference smooth wall data. ——, texture resolved DNS; - - -, textureless simulation using unsteady-Stokes admittance coefficients; $-\cdot-$, textureless simulation using using only $\mathscr{K}_{trsp}$ and slip length for $\boldsymbol{k} = [0,0]$ mode.

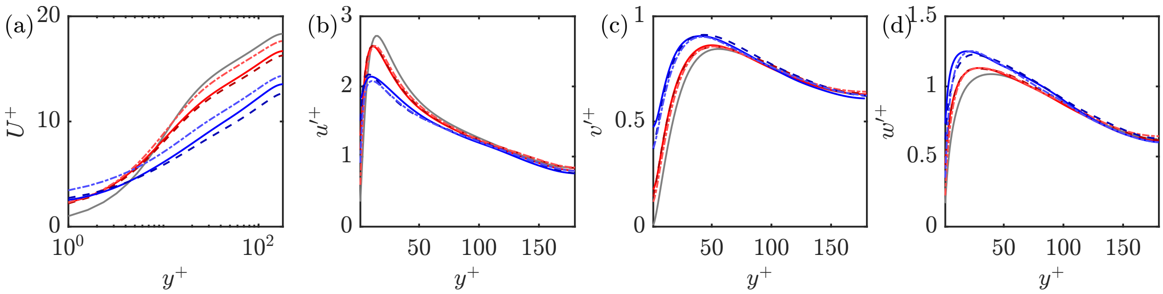

Figure 7. Mean flow and r.m.s velocity fluctuation profile of the simulation for rough textures. Lines are as in figure 6.

in equation 1 are selectively retained while all others are set to zero. This procedure allows us to isolate how the texture influences the overlying flow through distinct mechanisms, such as transpiration induced by pressure fluctuations or tangential velocity induced by shear. The slip length for the mean flow, $\boldsymbol{k} = [0,0]$, i.e. H_{uu} and H_{ww}, is kept in all cases, as it results in a Galilean translation which is critical for recovering the mean flow profile and ΔU^+, but does not otherwise affect the turbulence (Ibrahim *et al.*, 2021).

Simulations retaining any coefficient other than the pressure-driven transpiration coefficient H_{vp}, or equivalently, $\mathscr{K}_{trsp}$ in equation 2, become either numerically unstable or revert towards the smooth wall behaviour. Results from those keeping only $\mathscr{K}_{trsp}$ are included in figures 6 and 7. Overall, this model recovers the key trends in the profiles, with the r.m.s velocity fluctuations in close agreement with those obtained using the full set of unsteady-Stokes coefficients. Spectra for case Pd-48, representative of all cases here, are included in figure 8, and also exhibit good agreement with the DNS case. These observations are consistent with the findings of Hao & García-Mayoral (2025), where they argued that wall normal transpiration driven by pressure fluctuations is the primary mechanism for the changes in the drag and the overlying turbulence for the textures considered.

Focusing on the prediction of ΔU^+, the transpiration-only model yields errors of approximately 10% across most cases, comparable to the errors from simulations with the full set of coefficients. The only exception is the case Ro-24, where the discrepancy is significantly larger. The comparison between rough cases suggests that this higher error is associated with the shallower texture depth at smaller L^+. Hao & García-Mayoral (2025) argued that the proximity of the floor attenuates the transpiration effect, reducing the dominance of the $\mathscr{K}_{trsp}$ coefficient. In contrast, for the rough case with larger L^+, Ro-48, and the deep porous ones, the greater substrate depth supports a more active transpiration mechanism, leading to improved agreement with DNS when only this transpiration effect is retained. This suggests an increase with substrate depth in the dominance of transpiration driven by pressure.

Conclusions

In this work, we have first considered homogenisation methods to obtain admittance coefficients at the free-

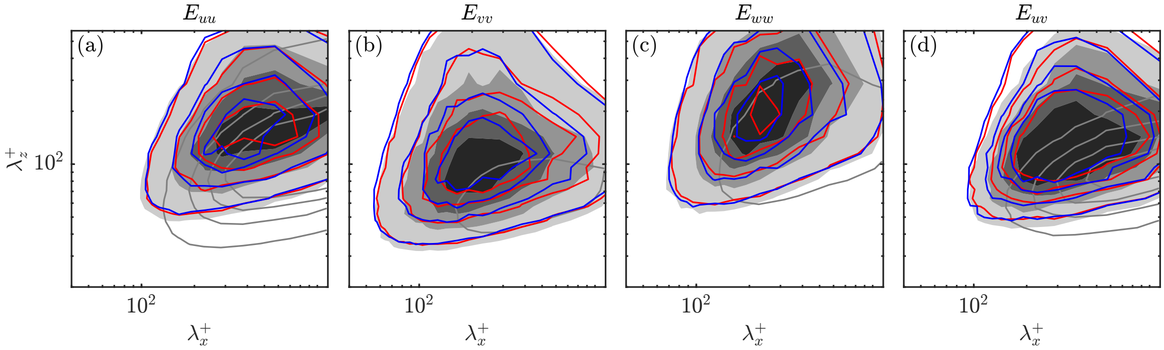

Figure 8. Premultiplied spectral energy densities at $y^+ = 15$ above the roughness tips for Pd-48 case. Shaded contours: texture-resolved DNS; ——, textureless simulation using unsteady-Stokes admittance coefficients; ——, $\mathscr{K}_{trsp}$ and slip length for uniform flow $\boldsymbol{k} = [0,0]$ only from unsteady-Stokes admittance coefficients; ——, reference smooth wall spectra. Contour levels are the same across the different cases.

flow/substrate interface. When the assumption of scale separation between the texture size and the lengthscales in the flow breaks, for $L^+ \lesssim 10$, the coefficients deviate significantly from the measurements of texture-resolved DNSs. We follow the proposed framework of Hao & Garcia-Mayoral (2022) and compute admittance coefficients using the flow response to finite-lengthscale excitations, considering the response flow as governed by either the steady or unsteady-Stokes equations. Comparison with coefficients extracted from texture-resolved DNS demonstrates that inertia, introduced in the form of temporal terms caused by the excitation travelling in the streamwise direction at wavespeed $c^+ = 10 - \Delta U^+$, is essential for obtaining accurate coefficients.

The resulting velocity-stress relationship is implemented as boundary conditions in simulations that do not explicitly resolve the texture. This approach successfully reproduces the key flow dynamics up to the largest texture size considered, $L^+ = 48$, though deviations increase with texture size. These results provide a practical route to modelling textured surfaces in turbulent flows without resolving the geometry, enabling simulations with much reduced cost. Further investigation is ongoing to establish the upper limit of texture size for which this methodology remains valid.

Through a systematic analysis where we retained alternatively one coefficient for textureless simulations, we showed that the pressure-driven transpiration effect plays the dominant role in modifying the turbulence for the textures considered, in agreement with findings by Hao & García-Mayoral (2025). For sufficiently deep porous and rough substrates, this transpiration effect, characterised by the coefficient $\mathscr{K}_{trsp}$, is sufficient to capture the effects of the texture on the turbulence. Ongoing work is examining whether transpiration coefficients at only a reduced set of lengthscales are enough to reproduce the flow dynamics. More broadly, a systematic assessment of the key coefficients for different texture types remains an open question for future study.

REFERENCES

Blackwelder, R. F. & Eckelmann, H. 1979 Streamwise vortices associated with the bursting phenomenon. *J. Fluid Mech.* **94** (3), 577–594.

Bottaro, A. & Naqvi, S. B. 2020 Effective boundary conditions at a rough wall: a high-order homogenization approach. *Meccanica* **55** (9), 1781–1800.

Del Álamo, J. C. & Jiménez, J. 2009 Estimation of turbulent convection velocities and corrections to Taylor's approximation. *J. Fluid Mech.* **640**, 5–26.

Fairhall, C. T., Abderrahaman-Elena, N. & García-Mayoral, R. 2019 The effect of slip and surface texture on turbulence over superhydrophobic surfaces. *J. Fluid Mech.* **861**, 88–118.

Gómez-de-Segura, G. & García-Mayoral, R. 2019 Turbulent drag reduction by anisotropic permeable substrates – analysis and direct numerical simulations. *J. Fluid Mech.* **875**, 124–172.

Hao, Z. & Garcia-Mayoral, R. 2022 Turbulent flows over porous/rough walls: Response of velocity to stress on surfaces. In *Bull. Am. Phys. Soc.*, , vol. 67.

Hao, Z. & García-Mayoral, R. 2025 Turbulent flows over porous and rough substrates. *J. Fluid Mech.* **1008**, A1.

Ibrahim, J. I., Gómez-de Segura, G., Chung, D. & García-Mayoral, R. 2021 The smooth-wall-like behaviour of turbulence over drag-altering surfaces: a unifying virtual-origin framework. *J. Fluid Mech.* **915**.

Kamrin, K., Bazant, M. Z. & Stone, H. A. 2010 Effective slip boundary conditions for arbitrary periodic surfaces: the surface mobility tensor. *J. Fluid Mech.* **658**, 409–437.

Lauga, E. & Stone, H. A. 2003 Effective slip in pressure-driven Stokes flow. *Journal of Fluid Mechanics* **489**, 55–77.

Luchini, P. 2013 Linearized no-slip boundary conditions at a rough surface. *J. Fluid Mech.* **737**, 349–367.

Luchini, P. & Chung, D. 2026 Higher-order homogenised riblet boundary conditions. *J. Fluid Mech.* **1030**, A2.

Luchini, P., Manzo, F. & Pozzi, A. 1991 Resistance of a grooved surface to parallel flow and cross-flow. *J. Fluid Mech.* **228**, 87–109.

Lācis, U., Sudhakar, Y., Pasche, S. & Bagheri, S. 2020 Transfer of mass and momentum at rough and porous surfaces. *J. Fluid Mech.* **884**, A21.

Naqvi, S. B. & Bottaro, A. 2021 Interfacial conditions between a free-fluid region and a porous medium. *Int. J. Heat Fluid Flow* **141**, 103585.

Sudhakar, Y., Lācis, U., Pasche, S. & Bagheri, S. 2021 Higher-Order Homogenized Boundary Conditions for Flows Over Rough and Porous Surfaces. *Transp. Porous Media* **136** (1), 1–42.

Xie, W., Fairhall, C. T. & García-Mayoral, R. 2024 Resolving turbulence and drag over textured surfaces using textureless simulations: the case of slip/no-slip textures. *J. Fluid Mech.* **1000**, A36.